# Energy Conversion Efficiency Enhancement of Polyethylene Glycol and a SiO₂ Composite Doped with Ni, Co, Zn, and Sc Oxides

Md. Hasan Zahir,* Mohammad Mizanur Rahman, Kashif Irshad, M. Nasiruzzaman Shaikh, Aasif Helal, Md. Abdul Aziz, Amjad Ali, and Firoz Khan

Read Online

ACCESS | Metrics & More | Article Recommendations | Supporting Information



PEG/Sc-SiO₂ PCM's thermal cycles represent high thermal stability

Energy conversion curves represent high storage efficiency
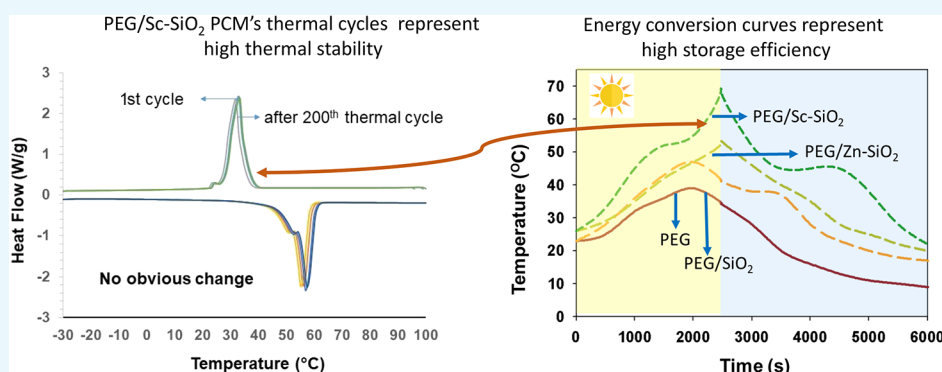
**ABSTRACT:** Doping the SiO₂ support with Co, Ni, Zn, and Sc improves the thermal conductivity of a hybrid PEG/SiO₂ form-stable phase change material (PCM). Doping also improves the energy utilization efficiency and speeds up the charging and discharging rates. The thermal, chemical, and hydrothermal stability of the PEG/Zn-SiO₂ and PEG/Sc-SiO₂ hybrid materials is better than that of the other doped materials. The phase change enthalpy of PEG/Zn-SiO₂ is 147.6 J/g lower than that of PEG/Sc-SiO₂, while the thermal conductivity is 40% higher. The phase change enthalpy of 155.8 J/g of PEG/Sc-SiO₂ PCM is very close to that of the parent PEG. PEG/Sc-SiO₂ also demonstrates excellent thermal stability when subjected to 200 consecutive heating–cooling cycles and outstanding hydrothermal stability when examined under a stream at 120 °C for 2 h. The supercooling of the PEG/Sc-SiO₂ system is the lowest among the tested materials. In addition, the developed PCM composite has a high energy storage capacity and high thermal energy storage/release rates.

## INTRODUCTION

Phase change materials (PCMs) should be highly efficient at converting light to heat, have a high thermal conductivity, and be stable. Additionally, an ideal system should have a low supercooling value and minimal leakage to ensure long-term performance. Owing to its high storage density and phase change temperature, polyethylene glycol (PEG) is one of the most promising PCMs for hot climates.[1,2] However, the low thermal conductivity of PEG and leakage issues associated with systems based on it are primary shortcomings in practical applications. Leakage problems associated with PEG can be overcome by encapsulating it in a matrix to create a form-stable composite phase change material (fs-CPCM) with the PEG polymer functioning exclusively within the matrix.[3−5]

Mesoporous silica is the most studied mesoporous material owing to its ability to precisely control the form, texture, and shape of the encapsulated material. Encapsulating a PCM in SiO₂ has been shown to improve its form stability.[6] Even though SiO₂-based PCMs have a high potential for solar thermal energy storage, UV−vis light does not interact directly

or effectively with them[7] due to their low thermal efficiency. Given that UV−vis light accounts for approximately 45% of the total solar energy,[8] harvesting it is critical for efficient solar energy conversion. Recently, we demonstrated that solar energy conversion efficiency (η) can be increased by incorporating organic PCMs in an inorganic support.[4] Although many materials selectively absorb visible light, collecting and converting full-band solar radiation are challenging.

Therefore, the primary objective of this study is the capture and transformation of full-band solar radiation. In this study, we have used four metal oxides, viz., NiO, Co₂O₃, ZnO, and Sc₂O₃, to enhance the absorption capabilities of SiO₂ in the

UV region. However, ZnO and $Sc_2O_3$ showed highly promising results. Studies have shown that ZnO has excellent chemical and thermal stability and that ZnO nanoparticles have a high absorption in the UV spectrum over a wide range of wavelengths.[9,10] At room temperature, ZnO behaves as a large-band-gap n-type semiconductor with a high excitation binding energy and strong excitation emission.[10] Additionally, ZnO is structurally stable, is morphologically controllable, and has a high excitation binding energy (60 MeV).[11] Optical measurements have revealed that even a small number of ZnO particles embedded in a $SiO_2$ matrix emit a bright light.[10,12] $Sc_2O_3$ exhibits strong photoluminescent properties with broad-band luminescence when exposed to UV light.[13] ZnO and $Sc_2O_3$ were combined with a $SiO_2$ matrix to form new PEG/Zn-SiO₂ and PEG/Zn-SiO₂ composites with enhanced full-band light-driven reversible phase transitions.

The properties of PEG/SiO₂ fs-thermal PCMs were compared with those of PCMs previously reported in the literature.[14] The enthalpy values of CPCMs prepared in this study are slightly lower than those reported in some reports,[14−20] while they are slightly higher than those reported in others.[15,18−20] The enthalpy of the PEG/SiO₂ composite made using oil shale ash (OSA) is higher than that of other phase change materials.[13,14] Owing to its high contamination with various toxic metal oxides, it is difficult to distinguish the source of thermal conductivity of $SiO_2$ obtained from OSA. Thus, the thermal conductivity values have not been provided.[14] Zhang et al.[21] reacted silica sheets with PEG at 70 °C for 4 h, yielding a PCM (PEG/silica sheet PCM) with a latent heat of 136.3 J/g. Wang et al.[22] found that PEG/silica fume composites have a latent heat of 81.3 J/g, which is very low when compared to that of PEG. This may be partly due to making the composites by mechanically mixing the components, which requires a series of complex silica fume pretreatment steps. Tang et al.[19,20] created an ss-PCM with a latent heat value of 168.84 J/g by mixing silica gel with PEG in the presence of methanol. Although the enthalpy of the composites improves, the absorption by materials with high porosity requires more energy and time. In addition, outgassing and drying processes of silica gel take a long time. Although several studies on solar energy storage using paraffin/SiO₂ and PEG/SiO₂ systems have been published, their many flaws remain and/or the results are questionable.

The main shortcomings of silica-based PCMs are their inability to maintain the structural integrity and low reliability under wet conditions, which are commonly encountered conditions in real-world applications. Hence, a hydrothermally stable PCM has a great potential for use in building applications. The morphology of silica changes when exposed to steam,[22,23] with small pores collapsing and larger pores expanding, results in a decrease of the selectivity of silica. Studies to overcome this shortcoming are worthwhile because $SiO_2$ is the preferred support for PCMs used for enhancing the comfort of occupants of buildings due to the outstanding working temperature range of silica, which is ideal for maintaining comfort levels in buildings in hot weather conditions.

Most of the reported PCMs have a weak thermal conductivity, which lowers the heat charging and discharging rates and decreases the thermal energy consumption efficiency. Researchers have investigated doping of the $SiO_2$ matrix with metal ions to increase the efficiency of microporous silica membranes.[23] The hydrothermal stability of composite oxides, including silica containing various metal ions such as Al, Mg, and Ni, is higher.[23−25] Researchers have doped $SiO_2$ with inorganic oxides, such as ZnO that has a thermal conductivity of 50 W/mK at room temperature, to improve the stability of silica support in the presence of steam and to enhance its thermal conductivity.[26] Zahir et al.[24] have discussed the utility of $Y_2O_3$-doped $SiO_2$ owing to their excellent characteristics, such as chemical stability and thermal conductivity. Sc and Y are members of the same group in the periodic table, and their chemical characteristics are similar to those of lanthanoids. Hence, Sc may play a dual role during network formation with $SiO_2$, making it worthwhile to look into the hydrothermal properties of Sc-doped $SiO_2$. Such a system can also help stabilize and prevent the aggregation of nanoparticles. Moreover, $Sc_2O_3$ can be a promising material for laser applications due to its high thermal conductivity and good absorption and/or emission properties.[13] In this study, five types of ss-PCMs were prepared using the parent $SiO_2$ and Co-, Ni-, Zn-, and Sc-doped $SiO_2$ with PEG, and their chemical and thermal stability and pore size distribution were evaluated. Thermal conductivity, solar energy conversion, and storage activity were also determined.

## ■ EXPERIMENTAL SECTION

**Materials.** The used PCM is polyethylene glycol with a molecular weight of 6000 that was purchased from Sigma-Aldrich Co., St. Louis, MO, USA. Ethyl alcohol was procured from BDH Chemicals Co. CNT was purchased from Cheap Tubes USA. $Zn(NO_3)_2 \cdot 6H_2O$ was purchased from Fisher Scientific Company, New Jersey, USA. $Sc(NO_3)_2 \cdot 6H_2O$, EthOH, $HNO_3$, and TEOS were purchased from Sigma-Aldrich Co., St. Louis, MO, USA.

## ■ SYNTHESIS

**Preparation of Composite PCMs and Selection of the Optimum Concentration of the Starting Materials.** Initially, $SiO_2$ and Sc-doped $SiO_2$ powder samples with varying Sc contents (Si/Sc = 2:1, 3:1, and 4:1) were synthesized using the sol−gel technique. Only the pore size distribution of Si/Sc (3:1) Sc-doped $SiO_2$ is not influenced by hydrothermal treatment, as indicated by its XRD pattern remaining similar to that of $SiO_2$. Recent research in the authors' laboratory indicates that the Y-doped $SiO_2$ membrane (Si/Y = 3:1) exhibits a stable performance.[24] Thus, data were collected for the Co-SiO₂, Ni-SiO₂, and Sc-SiO₂ samples with a Si to metal molar ratio of 3:1. In the case of Zn-SiO₂, however, this ratio cannot be achieved due to the minimal catalytic activity of Zn and because the loading in the system was very low. Synthesizing ordered mesoporous silica with a high Zn content is a difficult task. According to Cannas et al.,[27] ZnO nanocrystals can be introduced into mesoporous silica by impregnation using aqueous or ethanolic solutions of zinc nitrate. As the particles are bound in the rigid matrix of silica, the size of ZnO particles when embedded in $SiO_2$ does not change with the aging of the gel.

The following procedure was used to prepare Sc-doped silica sol with a Si/Sc ratio of 3:1. First, 8.34 g of TEOS was added to a solution containing a 50 g ethanol/11.49 g $Sc(NO_3)_2 \cdot 6H_2O$ mixture, which was hydrolyzed and condensed for 12 h. Afterward, water was added to get the total weight of the combination up to 500 g. By adding 2.0 g of $HNO_3$ to the sol, the pH was raised to 1.2, and the mixture was condensed for
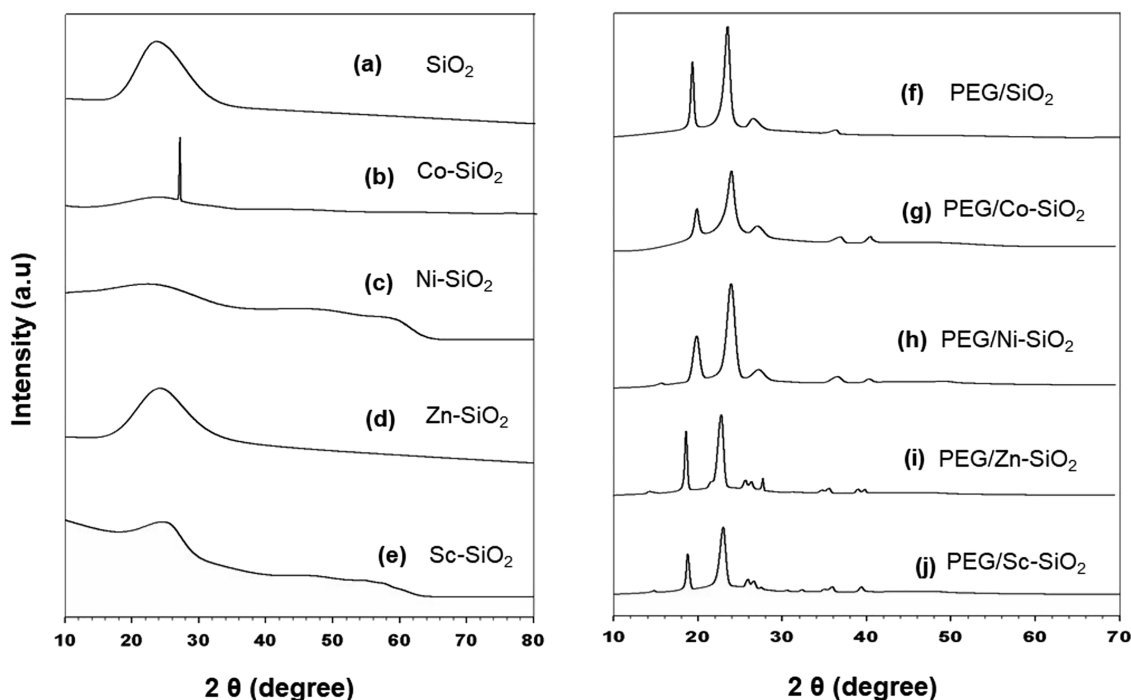
**Figure 1.** XRD patterns of (a) SiO$_2$, (b) Co-SiO$_2$, (c) Ni-SiO$_2$, (d) Zn-SiO$_2$, (e) Sc−SiO$_2$, (f) PEG/SiO$_2$, (g) PEG/Co-SiO$_2$, (h) PEG/Ni-SiO$_2$, (i) PEG/Zn-SiO$_2$, and (j) PEG/Sc-SiO$_2$ PCM simples.

another 12 h. Changing the catalyst amount, the water quantity, and the time of sol aging at room temperature can be used to control the degree of hydrolysis and condensation. The molar ratio of the components is 1:5.6:8:0.123 of TEOS/C$_2$H$_5$OH/H$_2$O/HNO$_3$.

**Composite PCM Preparation.** The SiO$_2$ and Co-, Ni-, Zn-, and Sc-doped SiO$_2$ with PEG PCM composite was synthesized by dissolving 0.5 g of PEG-6000 and 0.2 g of SiO$_2$ in 50 mL of ethanol with stirring for 30 min to mix the organic polymer and inorganic support well and allowing further dissolution by sonication for 30 min. Several composite PCMs with the composition PEG/Co-doped SiO$_2$, PEG/Ni-doped SiO$_2$, PEG/Zn-doped SiO$_2$, and PEG/Sc-doped SiO$_2$ were synthesized and characterized under the same above-mentioned procedure. The PCM was isolated by allowing the ethanol to evaporate at 80 °C for 24 h with stirring.

**Hydrothermal Treatment of the PCMs.** The importance of hydrothermal stability for a PCM when used for building applications, as noted above, is established. However, only a few studies have looked into the hydrothermal stability of SiO$_2$ supported PCM systems in the open literature. The PCMs were treated with water vapor in a Pyrex glass tubular reactor with an internal diameter of 12 mm. In the reactor, the samples were sandwiched between glass wool plugs. The gas flow rate was controlled with a mass flow controller, and the furnace temperature was increased at a linear heating rate. The PCM was converted into pellets, crushed, and sieved into 1−2 mm grains prior to conducting the stability tests in the presence of water vapor with a feed consisting of air and 10% water vapor in He.

**Characterization.** The XRD patterns were obtained by using a Bruker D8 advance diffractometer system (Berlin, Germany). The voltage at the operation point was set at 40 kV, and the current of the diffractometer was kept at 40 mA. The Cu Kα emission with monochromator graphite was at λ = 1.5405 Å. This information was gathered at a scan speed of 3 min$^{-1}$ and within the range of 2θ = 10−70°. Fourier transform infrared (FT-IR) spectra were recorded by the KBr pellet technique using a Bruker FT-IR spectroscope (Bruker AXS Analytical X-ray Systems GmbH, Berlin, Germany). Field emission scanning electron microscopy (FESEM; TESCAN LYRA3, Brno, Czech Republic) was used to define the size of particles and the products' morphology. The images were collected at a 10 kV acceleration voltage. Energy dispersive X-ray spectra (EDS) were obtained using an Oxford Instruments X-mass detector fitted to a Lyra3 TESCAN FESEM (JEOL USA Inc., Peabody, MA, USA). The diameter and volume of pores in addition to the specific surface area of the samples were determined by a NOVA-1200 device (JEOL USA Inc., Peabody, MA, USA). A Tristar II 3020 system was employed to define the BET surface area. The powders were evacuated for 3 h at 200 °C, and the experiments were applied at 5 °C/min from room temperature to 600 °C with a dry nitrogen atmosphere. The N$_2$ adsorption isotherms were obtained using liquid N$_2$ at a very low temperature, i.e., −196 °C. The distribution of pore sizes was determined using the Barrett−Joyner−Halenda isotherm. A Hitachi U-4100 spectrophotometer was used to record the UV−vis absorption spectra. The thermogravimetric analysis (TGA) of the samples was performed using a Shimadzu thermal analyzer (Tokyo, Japan, TA-50). The data of weight loss were gathered according to approximately 10 mg of a sample and at a heating rate of 5 °C/min from room temperature to 600 °C under a dry nitrogen flow. X-ray photoelectron spectroscopy (XPS) was used to define the chemical composition of the samples. In the same vein, an ESCALAB-250 (Thermo-VG Scientific, Waltham, Peabody, MA, USA) with Al Kα radiation (1486.6 eV) was employed. The XPS spectra were recorded at ambient temperature with a pressure of 5 × 10−10 mbar maintained in the specimen chamber. The samples' melting−freezing
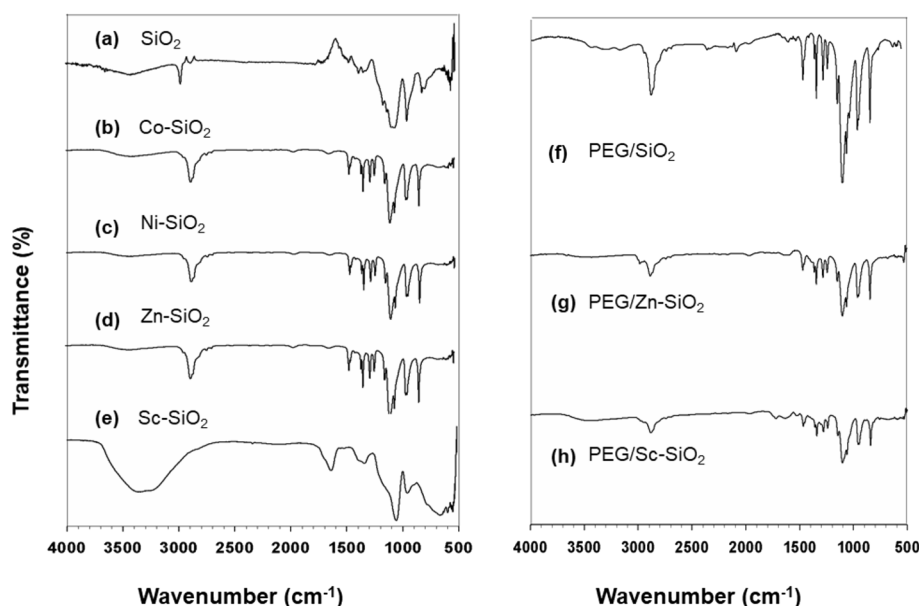
**Figure 2.** FTIR spectra of (a) $SiO_2$, (b) $Co-SiO_2$, (c) $Ni-SiO_2$, (d) $Zn-SiO_2$, (e) $Sc-SiO_2$, (f) $PEG/SiO_2$, (g) $PEG/Zn-SiO_2$, and (h) $PEG/Sc-SiO_2$ PCM simples.

points and the latent heat were determined using a DSC-Q2000. DSC data were gathered by heating 8.5 mg of sealed samples in an aluminum pan under an Ar gas flow rate of 20 mL/min at a heating rate of 5 °C/min. The Nanomaterials 2021, 11, 1639 5 of 24 thermal conductivity of the powders was determined with circular disk samples using a TCi Conductivity Analyzer, Canada. This equipment uses a modified transient plane source (MTPS) and the measurement method of C-Therm Technologies.

**Light-to-Heat Energy Conversion Experiment.** The experimental instruments and techniques for light to thermal conversion can be found in references 4 and 19. For irradiation, the samples (diameter 5 cm; mass 5.0 g) were placed in a heat-insulated foam container. A solar power meter was used to measure the strength of the radiation generated by the solar simulator (PlS-SXE300, Beijing Chang Tuo, China; TES-1333R, TES Electronic Corp., Taipei, Taiwan). The temperature−time curve was captured using a Pt thermocouple, a thermocouple-to-analogue connector (RS-232-RS-485, Instrument Co., Ltd., Jiangsu Suke, China), and a data logger (SK-130RD106062560021A1, Instrument Co., Ltd., Jiangsu Suke, China). On the PEG/Sc-SiO2 sample, a cyclic light irradiation experiment was performed. In the irradiation studies, simulated radiation with a power of 1000 W/m$^2$ was used to irradiate 19.6 cm$^2$ of a 5.0 g PCM sample placed in a weighing vial ($R$ = 2.5 cm). After 1 h of irradiation, the sample was turned off and allowed to cool to room temperature. The cycling tests were carried out 200 times. The hot and cold temperature zones are separated by a temperature gradient, often known as a thermocline.

■ **RESULTS AND DISCUSSION**

**Characterization of the Composite PCMs and Chemical Compatibility Analysis.** The XRD patterns of $SiO_2$ and Co-, Ni-, Zn-, and Sc-doped $SiO_2$ powders calcined at 120 °C in air for a duration of 24 h are shown in Figure 1. They are similar to the XRD pattern of silica, indicating that they are mostly amorphous materials. The XRD patterns of all samples have a broad band at a Bragg angle of $2\theta = 22°$ as

shown in Figure 1a, indicating that all samples mostly contain amorphous $SiO_2$ with a soft clay-type morphology. Mao et al. also observed the same phenomenon in the case of $Co-SiO_2$.[28]

A broadened XRD pattern was observed in the instance of $Ni-SiO_2$. All the samples except Co and Ni have 001 refractions, which are a good match to a basal spacing of about 4.5 nm. Multiple 001 refractions (d 002 and d 003) are observed for $SiO_2$, $Zn-SiO_2$, and $Sc-SiO_2$, suggesting a highly ordered layered structure. X-ray diffraction patterns of $SiO_2$, Zn-doped $SiO_2$, and Sc-doped $SiO_2$ are similar with only one unmatched broad peak, suggesting that these samples appear to be noncrystalline solids. Heat treatment of the samples up to 120 °C does not cause any unusual behavior except in the case of the $Co-SiO_2$ sample. The strong peak marginally moves toward higher diffraction angles in the case of $Sc-SiO_2$. This finding also implies that Sc-doped $SiO_2$ occurs as a noncrystalline material, viz., ultrafine particles undetectable by XRD.

After heat treatment at 120 °C, neither the Sc-based nanoparticles nor $SiO_2$ shows any signs of evolution. Hence, the samples are subjected only to a heat treatment at 120 °C for 24 h, which produces a lower number of defects typical for sol−gel silica. An intense silica gel diffraction peak and two sharp PEG diffraction peaks at 19.281 and 23.361 are seen in ss-PCMs, indicating that they have a composite structure made up of crystallite PEG and amorphous silica gel. Furthermore, despite the encapsulation of PEG within the pores of silica gel, discernible differences in the positions of the PEG peaks in the parent PEG and ss-PCM are not observed, showing that the crystal structure of PEG is not altered. The relative intensities of the peaks at 19.281 and 23.361 of ss-PCM are slightly lower than the theoretically predicted values, implying that silica gel interferes with PEG crystal formation. Furthermore, as the mass fraction of silica gel increases, the interference becomes stronger. The findings show that adding Co, Ni, Zn, or Sc to $SiO_2$ has no effect on the crystal structure of encapsulated PEG.

**FT-IR Spectroscopy.** FT-IR spectra of $SiO_2$ (Figure 2a), $Co-SiO_2$ (Figure 2b), $Ni-SiO_2$ (Figure 2c), $Zn-SiO_2$ (Figure
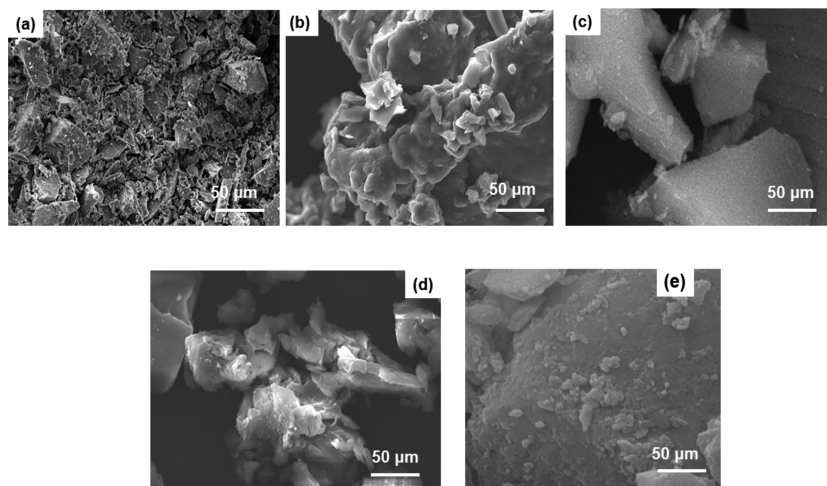
**Figure 3.** FE-SEM images of the as-synthesized (a) $SiO_2$, (b) Co-$SiO_2$, (c) Ni-$SiO_2$, (d) Zn-$SiO_2$, and (e) Sc-$SiO_2$.
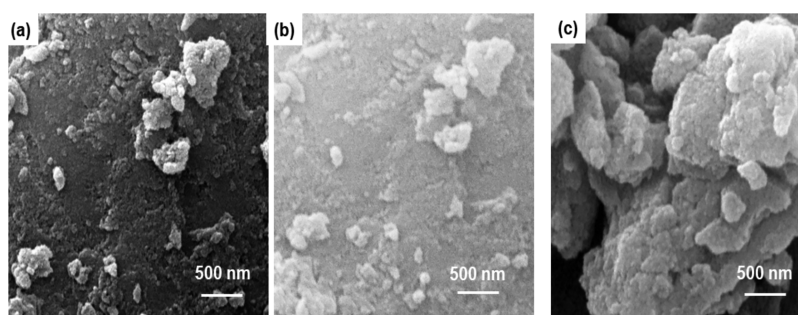


**Figure 4.** FE-SEM images of the as-synthesized (a) $SiO_2$, (b) Zn-$SiO_2$, and (c) Sc-$SiO_2$ powders at high magnification.

2d), and Sc-$SiO_2$ (Figure 2e) in the range of 4000 to 500 cm$^{-1}$ are shown in Figure 2. The peak of $\delta$SiO-H at 1636 cm$^{-1}$ has a slightly higher intensity in metal-containing $SiO_2$ than in $SiO_2$ alone. This may be because the metal precursors are strong oxidizers, converting the Si-OH group to SiH-O.[28] Most peaks in Sc-doped $SiO_2$ are broader than those of the other samples. In all samples, the characteristic of the Si−O−Si band is present at 803 cm$^{-1}$. The intensity of the peak of $SiO_2$ at 803 cm$^{-1}$ is higher than that of the other samples as shown by the spectra. Research shows that Si in Si−O−Si is substituted by Ni, Co, Ni, Zn, and Sc to form Si−O−X.[29] The shoulder peak observed at 669 cm$^{-1}$ in the metal-containing $SiO_2$ samples can be attributed to the Si−O−X (X = Ni, Co, Ni, Zn, and Sc) structural feature.[30]

In the FTIR spectra depicted in Figure 2f (PEG/$SiO_2$), Figure 2g (PEG/Zn-$SiO_2$), and Figure 2h (PEG/Sc-$SiO_2$), the peak at 1093 cm$^{-1}$ is attributed to the distortional vibrations of the Si-OH group. Two peaks that appear at 790 and 1061 cm$^{-1}$ are related to the Si−O−Si bond asymmetric and symmetric stretching vibrations, respectively. The spectra of ss-PCM show PEG peaks at 2888, 1468, 1344, 1114, 962, and 842 cm$^{-1}$, showing that PEG is encapsulated in the silica network. The O−H vibration, which indicates the presence of hydroxyl groups and/or adsorbed water, causes a peak in the range of 3150−3559 cm$^{-1}$.[31] The peaks between 800 to 1500 cm$^{-1}$ are due to the symmetric stretching vibration of the functional group of C−O−C. These peaks are shifted to a lower wavenumber, giving them a broad crab leg shape, while their intensity is slightly reduced, indicating a hydrogen bond between Si−OH and C−O−C of PEG.

The very intense absorption peaks at 841, 1359, 1468, and 2880 cm$^{-1}$ are attributed to CH$_2$ in the molecular chain of PEG. The plateau at 1094 cm$^{-1}$ is assigned to C−O−C.[31] In the spectra of the composites, the primary peaks attributable to characteristic functional groups of PEG and $SiO_2$ appear with just a little shift in peak locations and relative strength. The intermolecular hydrogen bonding between the Si−OH of silica and the hydroxyl groups of PEG is most likely responsible for this shift. The absence of extra peaks implies that the composite is made up of only PEG and $SiO_2$, indicating that chemical reactions do not take place and there are only physical interactions between PEG and the $SiO_2$ wall.

**Morphology.** Figure 3 shows the SEM images of $SiO_2$ (Figure 3a), Co-$SiO_2$ (Figure 3b), Ni-$SiO_2$ (Figure 3c), Zn-$SiO_2$ (Figure 3d), and Sc-$SiO_2$ (Figure 3e). The small particles of $SiO_2$ were observed, while the particles of Co-$SiO_2$, Ni-$SiO_2$, and Zn-$SiO_2$ have a similar morphology except that they are larger. Sc-$SiO_2$ has a wave-like morphology with a layered structure. Even though hydrolysis does not affect the platelets, they swell slightly more than those of $SiO_2$. In the case of Co- and Zn-doped samples, very few amorphous silica particles were observed in the vicinity of the platelets, implying that silica particles are rarely formed on the outside of clay-type platelets.[27]

At higher magnifications, $SiO_2$, Zn-$SiO_2$, and Sc-$SiO_2$ samples show soft-type nanosized particles (Figure 4). Figure 4a shows that the particles of $SiO_2$ are uniformly distributed. The average particle size of $SiO_2$, Zn-$SiO_2$, and Sc-$SiO_2$ is about 300 to 500 nm, with a homogeneous particle distribution as shown in Figure 4a−c. The EDS data obtained
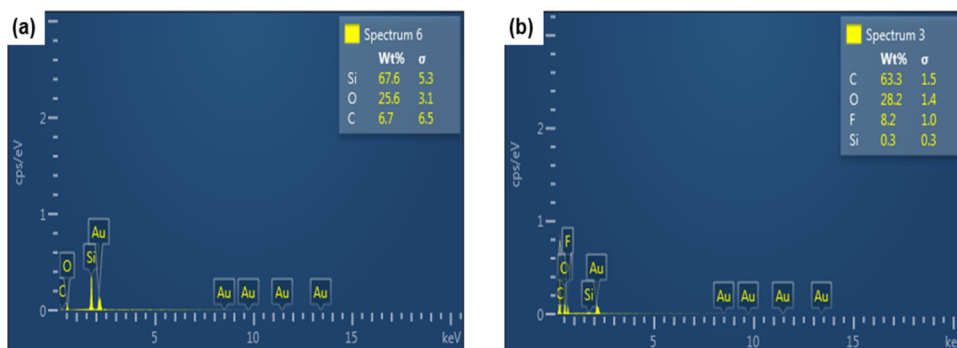
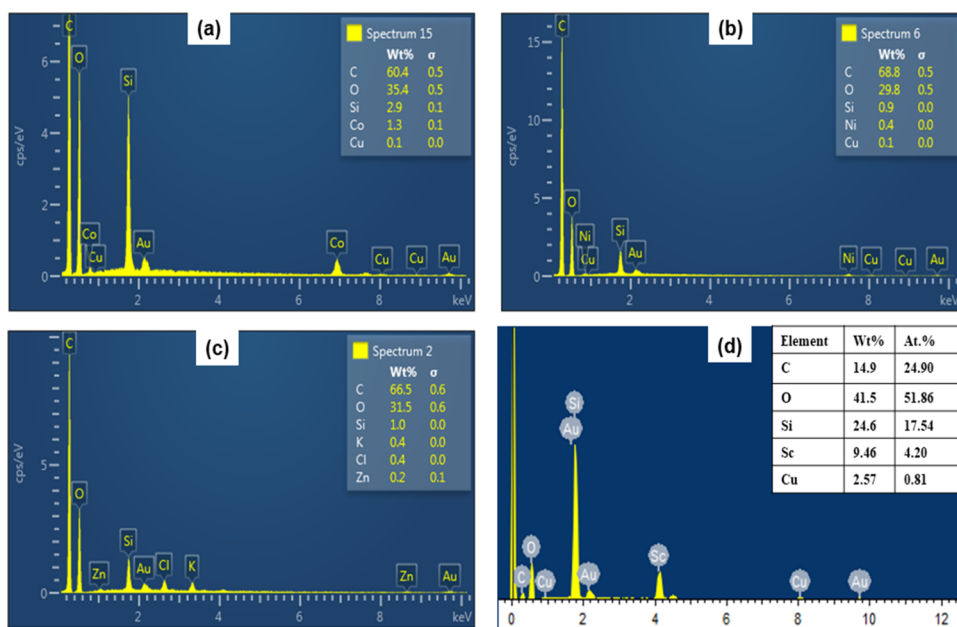**Figure 5.** Energy-dispersive spectra (EDS) of (a) $SiO_2$ and (b) PEG/$SiO_2$.



**Figure 6.** Energy-dispersive spectra (EDS) (a) PEG/Co-$SiO_2$, (b) PEG/Ni-$SiO_2$, (c) PEG/Zn-$SiO_2$, and (d) PEG/Sc-$SiO_2$.
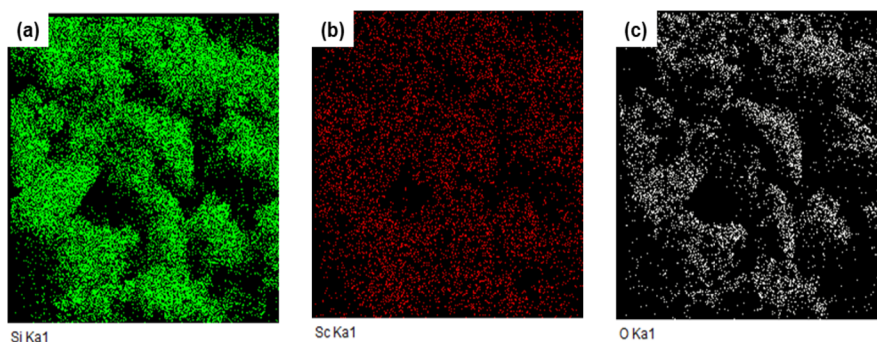


**Figure 7.** Mapping of a PEG/Sc-$SiO_2$ sample. The distribution represents (a) Si, (b) Sc, and (c) O elements.

from all points (Figures 5 and 6) reveal the presence of Si, C, and O in $SiO_2$, PEG/$SiO_2$, PEG/Co-$SiO_2$, PEG/Ni-$SiO_2$, PEG/Zn-$SiO_2$, and PEG/Sc-$SiO_2$. The EDS spectrum of PEG/Sc-$SiO_2$ shows strong peaks associated with the Si, O, and Sc atoms. The composition of samples corresponds to the elemental composition used in the preparation process. The lowest carbon weight percent among the tested samples was obtained for PEG/Sc-$SiO_2$, most likely due to the ability of Sc to scratch within the $SiO_2$ network. Determining the relative elemental ratio of Si/C/O accurately is difficult because of the

interference of the film of carbon formed on the copper grid and absorbed oxygen on the sample. The elemental maps of Sc-$SiO_2$ obtained using EDS, shown in Figure 7, indicate that the elements in the composite sample are evenly distributed with no obvious differences between them.

The surface elemental composition and valence state of Zn-$SiO_2$ samples were also determined using XPS spectra. According to the wide XPS spectrum in Figure S1, the composite materials were mostly made up of four elements: Zn, O, Si, and C. ZnO/$SiO_2$ showed characteristic binding
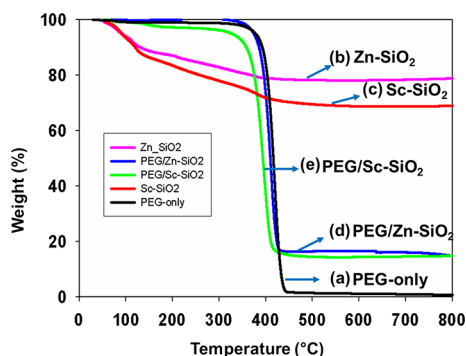
energy (B.E.) values of 1022.42 eV for Zn $2p_{3/2}$ and 1045.49 eV for Zn $2p_{1/2}$, indicating the existence of $Zn^{2+}$ in Zn-SiO$_2$ (Figure S1d). The binding energy of 1045.4 eV (Zn $2p_{3/2}$) found here was similar to that of Zn $2p_{3/2}$ in ZnO, showing that $Zn^{2+}$ existed in SiO$_2$ as ZnO. In the 99–100.5 eV range, the Si $2p_{1/2}$ and Si $2p_{3/2}$ lines agreed well with a divalent oxidation state for Si (Figure S1e). Furthermore, the high-resolution XPS spectrum of O 1s (Figure S1c) revealed an adsorbed oxygen signal at 531.1 eV. The conductive adhesive employed in the burning and testing of organic matter provided the majority of the C element.

**Thermal Stability.** The thermal stability of ss-PCM composites and PEG, which is considered the most important factor in applications involving thermal energy storage, is one of the critical parameters evaluated to assess the activity of ss-PCMs. Figure 8 shows the TGA curves of ZnO-SiO$_2$ (pink



**Figure 8.** TGA curves of (a) PEG-6000 (denoted by the black line), (b) Zn-SiO$_2$(denoted by the pink line), (c) Sc-SiO$_2$ (denoted by the red line), (d) PEG/Zn-SiO$_2$ (denoted by the blue line), and (e) PEG/Sc-SiO$_2$ (denoted by the green line).

line), Sc-SiO$_2$ (red line), PEG/Zn-SiO$_2$ (blue line), PEG/Sc-SiO$_2$ (green line), and PEG (black line). The TGA data were taken at a 5 °C/min heating rate in an argon environment.

The results in Figure 8 show that the decomposition that starts at room temperature is almost complete at about 600 °C. At 600 °C, the weight loss due to the removal of water and/or the decomposition of Zn-SiO$_2$ and Sc-SiO$_2$ is 20 and 32%, respectively. The weight loss of the matrix composite may have been caused by the elimination of absorbed water and hydroxyl groups from the matrix. The weight percentage of these composites remaining at 500 °C is about 18 and 17% for Zn-SiO$_2$ and Sc-SiO$_2$, respectively. The decomposition of PEG starts at about 350 °C and is completed (i.e., weight loss is 100%) at about 440 °C. Due to the elimination of the organic molecules, the weight loss of the composite occurs between 400 and 640 °C. PEG and PEG containing ss-PCM samples decompose in a single stage in the temperature range of 50 to 800 °C.

The inorganic porous support matrices of Zn-SiO$_2$ and Sc-SiO$_2$ seem to provide a protective shelter, which increases the thermal stability of PEG. The fabricated composites own a good thermal stability and thus are favorable for energy storage system applications. The results indicate that the Zn-SiO$_2$ and Sc-SiO$_2$ matrices inhibit the decomposition of encapsulated PEG. PEG/Zn-SiO$_2$ does not decompose in the temperature range of 25 to 390 °C, indicating that it is thermally stable up to 390 °C. Weight loss in the case of PEG/Sc-SiO$_2$ commences at about 140 °C, with the major weight loss starting at about 320 °C and completing at about 400 °C. PEG permeates through the silica gel pores, enhancing the formed ss-PCMs' thermal stability and allowing them to be employed over a wider temperature range. The thermal stability of silica gel networks, as well as intermolecular hydrogen bonding interactions between silica gel and PEG, contributes to the
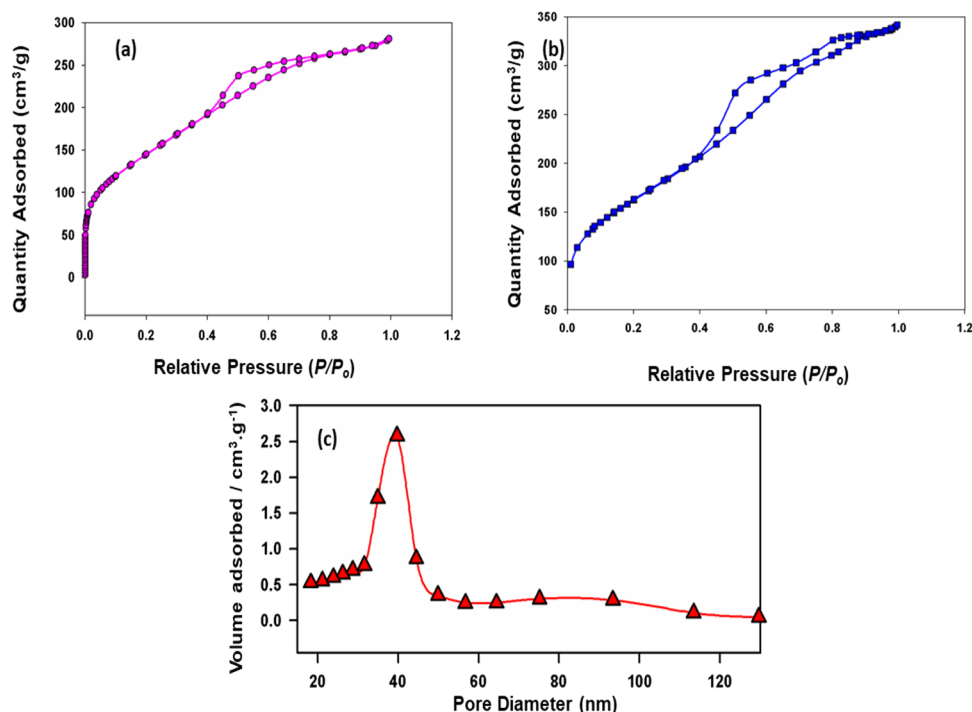


**Figure 9.** Nitrogen adsorption−desorption isotherms of the as-synthesized (a) Zn-SiO$_2$ and (b) Sc-SiO$_2$, and (c) the pore volume of Sc-SiO$_2$ powders.

improved stability. The initial breakdown temperature of silica gel composites is somewhat lower than that of PEG. As their starting decomposition temperatures are substantially greater than their phase change temperatures, ss-PCMs demonstrate excellent thermal durability well beyond the melting temperature range of a PCM based on PEG (330−350 °C). At temperatures below 263 °C, the PEG PCM possesses exceptional thermal stability characteristics, which are a key requirement in the use of PCM composites for heat storage applications.

**Pore Size Distribution.** The nitrogen adsorption−desorption isotherms of Zn-SiO$_2$ and Sc-SiO$_2$ powders are shown in Figure 9a,b. Both samples follow a typical type IV adsorption isotherm. The existence of a mesoporous structure, which is an ideal support material for ss-CPCMs, is shown by the hysteresis loops.[3,4] The pore size distribution is rather broad, as shown in Figure 9c, with somewhat uniform pore distributions. The surface area of Zn-SiO$_2$ and Sc-SiO$_2$ is 526.57 and 570.05 m$^2$/g, respectively, and the pore volume is 0.389 and 0.5767 cm$^2$/g, respectively. The improved PCM latent heat value of the Sc-SiO$_2$ based PCM matrix is probably due to its high pore volume capacity, which allows it to store a higher amount of PEG, in addition to the presence of mesopores.

**Thermal Storage Properties Determined by DSC.** The DSC curves for freezing and melting are shown in Figure 10a
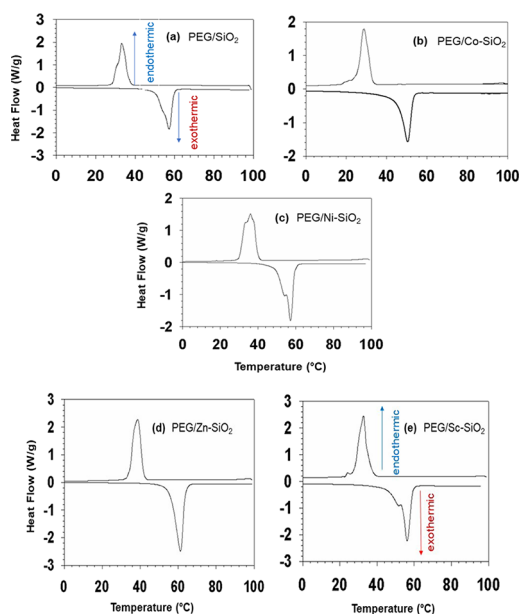


**Figure 10.** Melting−freezing DSC cycling curves of (a) PEG/SiO$_2$, (b) PEG/Co-SiO$_2$, (c) PEG/Ni-SiO$_2$, (d) PEG/Zn-SiO$_2$, and (e) PEG/Sc-SiO$_2$.

for PEG/SiO$_2$, Figure 10b for PEG/Co-SiO$_2$, Figure 10c for PEG/Ni-SiO$_2$, Figure 10d for PEG/Zn-SiO$_2$, and Figure 10e for PEG/Sc-SiO$_2$. The PEG and the composite system enthalpies were calculated by finding the total area below the DSC curves for freezing and melting cycles. The melting enthalpy of PEG is 189.6 J/g, while its freezing enthalpy is 170.1 J/g. The composite systems show a partial loss of the latent heat of both freezing and melting due to the presence of the matrix.

The PCMs based on the composites of (f) PEG/SiO$_2$, (g) PEG/Co-SiO$_2$, (h) PEG/Ni-SiO$_2$, (i) PEG/Zn-SiO$_2$, and (j)

PEG/Sc-SiO$_2$ exhibit an impregnation ratio ($R$) of 56.12, 57.01, 66.14, 77.93, and 82.17%, respectively (Table 2). This behavior can be explained by the composites' heterogeneous nature, in which PEG mixing, penetration, or both are less than ideal. This conclusion is supported by the weaker peaks of solidification and melting of the composites shown in Figure 10.

Table 2 also lists all the parameters calculated using the standard formulation,[22] where $T_m$ = melting temperature, $\Delta H_m$ = melting latent heat, $T_f$ = freezing temperature, $\Delta H_f$ = freezing latent heat, $\Delta T_s$ = supercooling, $R$ = impregnation ratio, and $E$ = impregnation efficiency. The results reported for a few PCMs of the type similar to those investigated in this study are also included in Table 2 for comparison purposes.

$$E_{eff} = \frac{\Delta H_m, \text{PCM}}{x_{PEG}} \quad (1)$$

$$R = \frac{\Delta H_m, \text{com}}{\Delta H_m, \text{PCM}} \times 100\% \quad (2)$$

$$E = \frac{\Delta H_m, \text{com} + \Delta H_f, \text{com}}{\Delta H_m, \text{PCM} + \Delta H_f, \text{PCM}} \times 100\% \quad (3)$$

In eqs 1−4, com = OA, SC, or ExP matrix and PCM = matrix + PEG.

The results indicate that PEG/Zn-SiO$_2$ and PEG/Sc-SiO$_2$ perform better with an impregnation efficiency of 77.93 and 82.17%%, respectively, compared to other samples. Moreover, the impregnation efficiency ($E$%) of PEG/Zn-SiO$_2$ and PEG/Sc-SiO$_2$ is also better, as Table 1 shows. The thermal storage capacity of the PEG/Sc-SiO$_2$ composite indicates that practically all PEG molecules release/store energy efficiently during phase transitions. As a result, a higher latent heat value of 155.8 J/g was obtained, which is higher than that of the other tested samples. This value is also comparatively higher than the reported values shown in Table 1.

The findings of this study are also comparable to those reported for other ss-PCMs (Table 1). Despite the fact that many organic and inorganic PCMs have a high latent heat of combustion, researchers have mainly investigated PCMs with paraffin and those that are PEG-based as they have an ideal working temperature range for providing comfort in buildings, particularly in hot climates. In addition, the tested PCMs have a high energy storage efficiency, with the highest value of 96.48%, which is an important evaluation parameter. The efficiency values obtained for the materials investigated in the current study are better compared to those reported in previous works (Table 1). The extent of supercooling $\Delta T_s$, obtained based on the solidification and melting temperature difference of (a) PEG, (b) PEG/SiO$_2$, (c) PEG/Co-SiO$_2$, (d) PEG/Ni-SiO$_2$, PEG/Zn-SiO$_2$, and PEG/Sc-SiO$_2$, is 24.98, 22.63, 21.96, 21.45, 20.64, and 19.00 °C, respectively. The largest reduction in supercooling of 25.5% is obtained for the PEG/Sc-SiO$_2$ composite. The XRD patterns shown in Figure 1 indicate that PEG/Sc-SiO$_2$ has the largest decrease in peak height among the five PCMs compared to that of PEG. The results indicate that a larger portion of PEG is encapsulated in the porous structure of PEG/Sc-SiO$_2$ compared to PEG/SiO$_2$, PEG/Co-SiO$_2$, PEG/Ni-SiO$_2$, and PEG/Zn-SiO$_2$. The higher solidification and melting latent heats of PEG/Sc-SiO$_2$ support this conclusion. Moreover, the lack of any vapor/gas formation during the melting cycle is noteworthy. Furthermore, no

**Table 1. Thermal Activities of PEG, PEG/SiO$_2$, Co/PEG/SiO$_2$, Ni/PEG/SiO$_2$, Zn/PEG/SiO$_2$, and Sc/PEG/SiO$_2$ Composites and Comparison with That of PEG/SiO$_2$ in the Literature[a]**

| samples | $T_f$ (°C) | $T_m$ (°C) | $H_f$ (J/g) | $H_m$ (J/g) | $\Delta T$ (°C) | $R$ (%) | $E$ (%) | $\Phi$ (%) | $\gamma$ (%) | references |
|---|---|---|---|---|---|---|---|---|---|---|
| PEG | 38.04 | 63.02 | 170.1 | 189.6 | 24.98 | | | | 100 | this work |
| PEG/SiO$_2$ | 33.02 | 55.65 | 104.5 | 106.4 | 22.63 | 56.12 | 58.63 | 104.48 | 78.57 | this work |
| PEG/Co-SiO$_2$ | 28.61 | 50.57 | 104.7 | 108.1 | 21.96 | 57.01 | 59.16 | 103.76 | 73.30 | this work |
| PEG/Ni-SiO$_2$ | 35.85 | 57.30 | 118.9 | 125.4 | 21.45 | 66.14 | 67.92 | 102.69 | 99.21 | this work |
| PEG/Zn-SiO$_2$ | 38.60 | 59.24 | 139.9 | 147.6 | 20.64 | 77.93 | 79.93 | 102.67 | 108.99 | this work |
| PEG/Sc-SiO$_2$ | 33.01 | 52.01 | 153.1 | 155.8 | 19.00 | 82.17 | 85.17 | 104.51 | 105.65 | this work |
| PEG/SiO$_2$ | 44 | 59 | 105.1 | 171 | 15 | | | | | Tang, B (2013)[20] |
| PEG/SiO$_2$ | 23.3 | 36 | 118.3 | 122 | 12.7 | | | | | He, L (2014)[16] |
| PEG/SiO$_2$/Cu | 45.8 | 58.2 | 102.8 | 100.4 | 12.4 | | | | | Tang, B (2012)[18] |
| PEG/SiO$_2$/Al$_2$O$_3$ | 42 | 57.1 | 126.4 | 123.8 | 15.1 | | | | | Tang, B (2014)[19] |
| PEG/SiO$_2$ | - | 61.6 | - | 162.9 | - | | | | | Wang, W (2009)[22] |
| PEG/SiO$_2$ | 42.34 | 58.09 | 141 | 151.8 | 15.75 | | | | | Qian, T (2015)[14] |
| PEG/SiO$_2$ | 37.3 | 52.2 | 173.3 | 172.9 | 14.9 | | | | | Yang, J (2019)[32] |
| PEG/SiO$_2$ | 37.9 | 60.4 | 160.1 | 164.9 | 22.5 | | | | | Li, B (2020)[15] |
| PEG/SAM-4 | 39 | 59.5 | 113.5 | 116.3 | 20.5 | | | | | Yan, D (2021)[33] |

[a]$T_f$ = freezing temperature, $T_m$ = melting temperature, $\Delta H_f$ = latent heat in the cooling process, $\Delta H_m$ = latent heat in the heating process, $\Delta T$ = supercooling, $E_{ef}$ = efficient energy per unit mass of PEG, $R$ = impregnation ratio, $E$ = energy storage efficiency, $\varphi$ = energy storage capacity, and $\gamma$ = heat storage efficiency. This study represents the present study, and (-) = data not available. The maximal deviation determined for phase change temperature and latent heat is ±0.10 °C and ±0.42 J/g, respectively, taking into account the averages of three measurements.

cavities are formed during the freezing process. That is why the PEG/Sc-SiO$_2$ PCM was stable even after 200 thermal cycles as discussed below.

**Thermal Conductivity of the PCMs Based on PEG/SiO$_2$ Composites.** As heat transfer is faster at higher density, the increased thermal conductivity of PEG/Zn-SiO$_2$ is most likely due to its higher density. Hence, the presence of Zn-SiO$_2$ in the PCM composite significantly improves the thermal conductivity while maintaining the compatibility, thermal stability, or TES properties of the PCM the same.

Even after allowing for the differences in the synthetic procedure, ambiguities among the reported results still exist. The latent heat value of melting of the PEG/SiO$_2$/graphite system is very low at 128.4 J/g. As the thermal conductivity of ZnO is calculated to be 50 W/mK at room temperature, adding ZnO improves the thermal conductivity of PEG/SiO$_2$. In fact, the thermal conductivity of PEG/Zn-SiO$_2$ is higher than that of PEG or SiO$_2$ alone, and ZnO-doped SiO$_2$ is expected to serve as an excellent matrix. Therefore, combining these two inorganic materials provides a suitable matrix for ss-PCM applications. The thermal conductivity of PEG/ZnO-SiO$_2$ and PEG/Sc-SiO$_2$ determined in this study is 0.6532 and 0.5731 W/mK, respectively (Table 2). The improvement of the thermal conductivity of PEG/Zn-SiO$_2$ is most likely due to the presence of highly conductive ZnO inside the thermally conductive SiO$_2$ network, which probably enhances the intermolecular forces. The uniform distribution of Zn oxide particles in PEG/Zn-SiO$_2$ compared to the other composites also contributes to the higher thermal conductivity of the Zn composite. The enhancement of PEG/Sc-SiO$_2$ conductivity is substantially higher compared to that of PEG/Cu-SiO$_2$.[18] For the sake of comparison, we have included several thermal conductivity data in Table 2. Graphene-containing samples had good conductivity; however, graphene is an expensive material.

**Compatibility of PCM with Containers.** As the synthesized PCMs have to be stored in suitable containers for future use, their compatibility with several metals used to fabricate containers was evaluated. For this purpose, sheets of copper, aluminum, zinc, stainless steel, and galvanized iron

**Table 2. Thermal Conductivity of PEG, Zn/PEG/SiO$_2$, and Sc/PEG/SiO$_2$[a]**

| material | thermal conductivity (Wm$^{-1}$ k$^{-1}$) | reference |
|---|---|---|
| PEG | 0.23 | this work |
| PEG/Zn-SiO$_2$ | 0.6532 | this work |
| PEG/Sc-SiO$_2$ | 0.5731 | this work |
| PEG/SiO$_2$ | 0.5581 | Li, J (2013)[17] |
| PEG/Cu-SiO$_2$ | 0.4141 | Tang, B (2012)[18] |
| PEG/SiO$_2$ | 0.5124 | Wang, W (2009)[22] |
| PEG/SAM-4 | 0.48 | Yan, D (2021)[33] |
| octadecanol/graphene oxide | 4.28 | Yang, J (2018)[35,36,38] |
| octadecanol/graphene nanoplatelets | 4.28 | Yang, Y (2018) |
| PEG/graphene | 1.35 | Yang, Y (2016) |
| paraffin/graphene acrogel | 2.68 | Min, P (2018)[37] |

[a]The measured maximal deviations for conductivity values were ±0.05 Wm$^{-1}$ k$^{-1}$ taking into account the averages of the five measurements for these study data.

shown in Figure 11a−e, respectively, were coated with the relevant PCM and exposed to atmospheric conditions. Figure 11 shows metal sheets coated with PEG/SiO$_2$ (a′, b′, c′, d′, and e′), PEG/Zn-SiO$_2$ (a″, b″, c″, d″, and e″), and PEG/Sc-SiO$_2$ (a‴, b‴, c‴, d‴, and e‴) after 4 months of exposure to atmospheric conditions (June to September, with the highest temperature of about 50 °C and the lowest of about 15 °C).

The PCM specimens were placed on the metal sheets, and their surface properties were characterized after exposure under atmospheric conditions of high solar radiation and humidity for 4 months. The color of Cu, Al, Zn, stainless steel, and galvanized iron sheets that were in contact with PEG/Zn-SiO$_2$ and PEG/Sc-SiO$_2$ PCMs did not change, indicating that the metal substrate was not affected by these two ss-PCMs. Also, the weight of the specimens did not change due to atmospheric exposure. However, the color of the PEG/SiO$_2$ PCM sample placed on the Cu sheet changed slightly, indicating that a container made of Cu is not suitable to
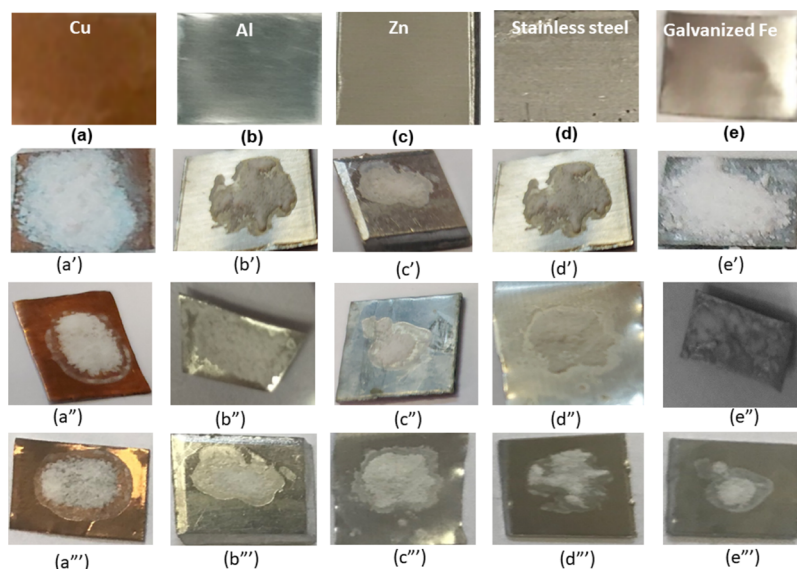
**Figure 11.** Photographs of compatibility tests of (a) copper, (b) aluminum, (c) zinc, (d) stainless steel, and (e) galvanized iron metal sheets coated with $SiO_2$ (first row: a′, b′, c′, d′, and e′), Zn-$SiO_2$ (second row: a″, b″, c″, d″, and e″), and Sc-$SiO_2$ (third row: a‴, b‴, c‴, d‴, and e‴) after 5 months of exposure at atmospheric conditions (highest temperature May to September, 50 °C; lowest temperature, 10 °C).

store the PEG/$SiO_2$ PCM. Thus, the results indicate that PEG/Zn-$SiO_2$ and PEG/Sc-$SiO_2$ are compatible with aluminum, zinc, stainless steel, and galvanized iron, and as such, these metals can be used to fabricate containers for long-term storage of the synthesized PCMs.

**Seepage Test (Leakage Test).** PEG (Figure 12a), Sc-$SiO_2$ (Figure 12b), and PEG/Sc-$SiO_2$ PCM (Figure 12c) each were compressed into a disk of 20 mm diameter and placed on a filter paper on a laboratory heating platform.
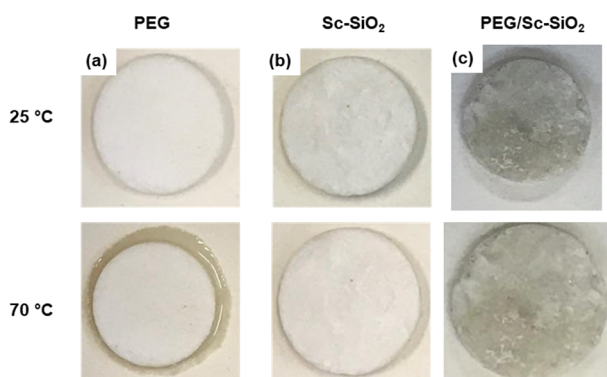


**Figure 12.** Photographs of (a) PEG, (b) Sc-$SiO_2$, and (c) PEG/Sc-$SiO_2$ at 25 °C (upper row) and after being heated at 70 °C (lower row) for leakage checking (see page test).

As the images in Figure 12 show, melting is not visible in the PEG/Sc-$SiO_2$ composite, indicating that PEG leakage is absent even after heating the disk at 70 °C for 10 min, whereas PEG starts to melt when heated to 70 °C. As demonstrated in Figure 12, the color shift rates of PEG/Sc-$SiO_2$ are different, implying that its heat transfer rates are different. After 10 s, PEG/Sc-$SiO_2$ demonstrates the fastest color change representing the fastest temperature shift, which indicates that PEG/Sc-$SiO_2$ has the maximum thermal conductivity. A careful observation has been conducted to each filter paper after each sample has been removed from the corresponding filter paper.

**Thermal Recycling Properties of the PEG/Sc-$SiO_2$ Composite PCM.** Some of the DSC data for PEG/Sc-$SiO_2$ subjected to 200 thermal cycles are depicted in Figure 13. As shown in Figure 13a, both exothermic and endothermic peaks do not change due to thermal cycling, indicating that the composite has a long life cycle and high thermal stability. These DSC findings indicate that, in terms of temperature and enthalpies, the PEG/Sc-$SiO_2$ composite can maintain nearly constant phase changes. Hence, this system can be utilized to store and release latent heat in applications involving repeated heating/cooling cycles at a consistent temperature.

The PEG/Sc-$SiO_2$ PCM retains its shape after undergoing reversible phase shift during cyclic heating and cooling experiments. Capillary action and surface tension associated with the silica nanoporous structure limit the leakage of PEG, which explains this behavior. The FE-SEM image obtained after 200 thermal cycles depicted in Figure 13b shows that PEG/Sc-$SiO_2$ PCM can maintain its structure even when subjected to vigorous thermal cycling. Even after 200 cycles, extra peaks are not observed in the DSC curves, and only minor shifts of the peaks in the melting and freezing curves are observed. A careful study of the FE-SEM image reveals that the Sc-$SiO_2$ and PEG particles are well mixed. The laminated structure of PEG/Sc-$SiO_2$ provides an excellent support for PEG and Sc nanoparticles. Cheng et al. have reported that PEG is typically present in the pores of the associated PCM matrices.[34] In the ss-PCM, PEG fills the pores in the $SiO_2$ network, confirming the quasi-uniform distribution of PEG. The characteristic peaks in the FTIR spectrum of PEG/Sc-$SiO_2$ after 200 thermal cycles remain nearly unchanged, indicating that the structure of PEG/Sc-$SiO_2$ is chemically stable when subjected to thermal cycling. This indicates that the prepared PEG/Sc-$SiO_2$ composite PCM is structurally and chemically stable, which is beneficial for applications in providing comfort in buildings. Also, the XRD patterns before and after hydrothermal treatment remain unchanged, indicating that PEG/Sc-$SiO_2$ is stable at 200 °C in the presence of 10% water vapor.
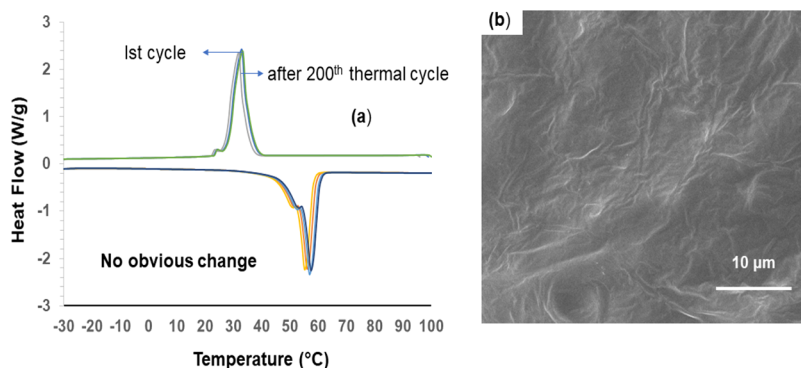
**Figure 13.** (a) Melting−freezing DSC cycling curves of the PEG/Sc-SiO$_2$ PCM sample repeated 200 times and (b) SEM image of the sample after the 200th cycle.
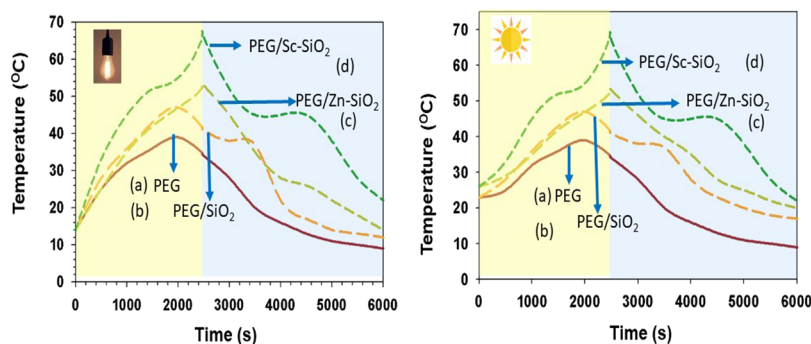


**Figure 14.** Left image: light-to-thermal energy conversion curves of (a) PEG and (b) PEG/SiO$_2$, (c) PEG/Zn-SiO$_2$, and (d) PEG/Sc-SiO$_2$ composites under solar simulator radiation ($I$ = 120 mWcm$^{-2}$). Right image: solar-to-thermal energy conversion curves of (a) PEG and (b) PEG/SiO$_2$, (c) PEG/Zn-SiO$_2$, and (d) PEG/Sc-SiO$_2$ composites under irradiation with sunlight ($I$ = 98 mWcm$^{-2}$, 12:00 to 13:55 h, June 13th, 2021).
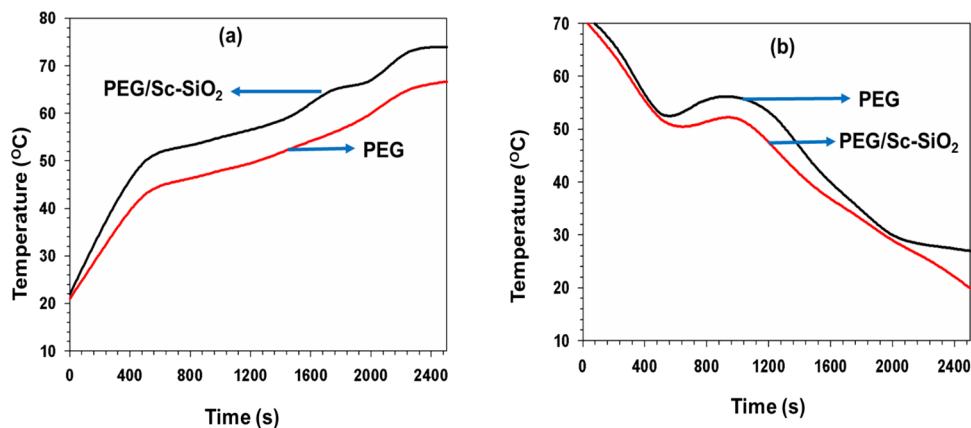


**Figure 15.** (a) Heating and (b) freezing temperature curves of PEG and the PEG/Sc-SiO$_2$ composite.

**Solar-to-Thermal Energy Storage Efficiency.** Owing to its favorable optical properties, the PEG/Sc-SiO$_2$ PCM can also be used for solar-to-thermal conversion and TES. PEG/Sc-SiO$_2$ nanoparticles, the porous structure of Sc-SiO$_2$, or both improve the PEG light absorption throughout the bandwidth; in addition, the absorption increased at around ∼240 and ∼300 nm (Figure S2). The enhanced full-band absorption and selective absorption afford the PEG/Sc-SiO$_2$ composite excellent photothermal conversion efficiency. The intensity of the absorption peaks in the UV−vis spectra of PEG/Sc-SiO$_2$ is higher compared with that of pure PEG. Solar energy conversion into thermal energy and the energy storage capacity of PCMs may be computed simultaneously using the present technique, which takes into account the high latent heat and good optical characteristics of PCMs.[4] Also, PEG/Sc-SiO$_2$ absorbs higher light higher compared with pure PEG across the whole visible region. Several temperature recorders were placed under the solar simulators to evaluate the conversion of solar energy into thermal energy by PEG and PEG/Sc-SiO$_2$. Figure 14 implies a temperature rise, which may be assigned to the good activity of Sc-SiO$_2$ and/or PEG due to the photon emission and the formation of molecular stoves. The PEG temperature increases according to the increase of infrared light in solar radiation. A peak value was obtained after long-term radiation exposure, demonstrating the storage of thermal energy via a phase change. A cooling stage is present in the cooling process due to the release of energy.

The PCM composite is heated by thermal energy, which is held by the composites due to phase transitions in the PCMs. The solar-to-thermal energy storage efficiency ($\eta$) in the visible region has been calculated using eq 4:

$$\eta = \frac{m\Delta H}{IS(T_t - T_f)} \tag{4}$$

where $m$ refers to the sample weight, $\Delta H$ is the melting phase change, $I$ is the power density, $S$ is the radiated field, and $T_t$ and $T_f$ are related to the start and end transition time points of the phases. The solar efficiency values of samples (b) PEG/SiO$_2$, (c) PEG/Zn-SiO$_2$, (d) and PEG/Sc-SiO$_2$ in Figure 14 are 60.6, 64.7, and 75.5%, respectively. Compared to the results reported for carbon-based PCMs, these results show that photothermal energy can be stored effectively. According to Cheng et al.,[34] a PCM based on a wax coated with carbon nanotubes has a heat storage efficiency of 40 to 60%. The PEG/Sc-SiO$_2$ PCM was exposed to sunlight to simulate its activity in an actual application and to evaluate its performance. The temperature of the PCM increased after prolonged exposure under solar light, and an optimum value was obtained for increasing and decreasing temperature, as shown in Figure 14d. This device can store energy and converts energy through a phase transformation from solar to heat. The high PEG/Sc-SiO$_2$ enthalpy values show that the manufactured PCM has a large thermal capacity to fulfill the demands of real applications. Furthermore, the solar-to-thermal energy conversion curves are shown in Figure 15a,b. The melting and freezing temperature curves are clearly comparable to the plateau heating and cooling temperatures, as seen in these graphs. The solar-to-thermal conversion efficiency after 200 cycles was reduced by a percent of only 0.49%.

## CONCLUSIONS

FT-IR spectra and XRD patterns of PEG/Sc-SiO$_2$ before and after cycling are nearly identical, indicating that the chemical and crystal structures of the PCM are not altered. The differences among PEG/SiO$_2$, PEG/Zn-SiO$_2$, and PEG/Sc-SiO$_2$ and their performance enhancement were demonstrated. DSC and TGA were used to validate the thermal properties and thermal stability of the composite PCM. The melting and freezing latent heat values of PEG/Sc-SiO$_2$ before subjecting to thermal cycling are 155.8 and 153.1 J/g, respectively, while after cycling, they are 153.0 and 152.0 J/g, respectively. Hence, melting and freezing latent heat decreases by negligibly small amounts of 2.4 and 2.9% when the PCM is subjected to thermal cycling for 200 times. The light-to-heat conversion and energy storage capability of the PCM were also evaluated. PEG/Sc-SiO$_2$ remains thermally and chemically stable when subjected to prolonged irradiation, indicating that PEG/Sc-SiO$_2$ has excellent reversibility and can be used repeatedly for applications involving energy storage. The outstanding advantages, namely, higher latent heat values, low super-cooling, excellent charging/discharging rates, high conversion values, and the unique hydrothermal stability, indicate that the fabricated PCMs have a high potential. In this study, porous materials with improved energy storage capability were synthesized, and a general method for increasing the loading of PCMs in porous materials was elucidated.

## ASSOCIATED CONTENT

### ⓢ Supporting Information

The Supporting Information is available free of charge at https://pubs.acs.org/doi/10.1021/acsomega.2c02107.

XPS spectra of Zn-SiO$_2$ (Figure S1) and UV−vis adsorption spectra of PEG (blue line), PEG/SiO$_2$ (black line), PEG-Zn-SiO$_2$ (red line), and PEG-Sc-SiO$_2$ (green line) (Figure S2) (PDF)

## AUTHOR INFORMATION

### Corresponding Author

**Md. Hasan Zahir** − *Interdisciplinary Research Center for Renewable Energy and Power Systems (IRC-REPS), Research Institute, King Fahd University of Petroleum & Minerals, (KFUPM), Dhahran 31261, Saudi Arabia;* ⓘ orcid.org/0000-0002-6752-9318; Email: hzahir@kfupm.edu.sa

### Authors

**Mohammad Mizanur Rahman** − *Interdisciplinary Research Center for Advanced Materials, KFUPM, Dhahran 31261, Saudi Arabia;* ⓘ orcid.org/0000-0002-9302-3185

**Kashif Irshad** − *Interdisciplinary Research Center for Renewable Energy and Power Systems (IRC-REPS), Research Institute, King Fahd University of Petroleum & Minerals, (KFUPM), Dhahran 31261, Saudi Arabia; Researcher at K.A.CARE Energy Research & Innovation Center, Dhahran 31261, Saudi Arabia;* ⓘ orcid.org/0000-0001-6493-0969

**M. Nasiruzzaman Shaikh** − *Interdisciplinary Research Center for Hydrogen and Energy Storage, KFUPM, Dhahran 31261, Saudi Arabia;* ⓘ orcid.org/0000-0002-9549-6322

**Aasif Helal** − *Interdisciplinary Research Center for Hydrogen and Energy Storage, KFUPM, Dhahran 31261, Saudi Arabia;* ⓘ orcid.org/0000-0003-2013-5327

**Md. Abdul Aziz** − *Interdisciplinary Research Center for Hydrogen and Energy Storage, KFUPM, Dhahran 31261, Saudi Arabia;* ⓘ orcid.org/0000-0002-1537-2785

**Amjad Ali** − *Interdisciplinary Research Center for Renewable Energy and Power Systems (IRC-REPS), Research Institute, King Fahd University of Petroleum & Minerals, (KFUPM), Dhahran 31261, Saudi Arabia*

**Firoz Khan** − *Interdisciplinary Research Center for Renewable Energy and Power Systems (IRC-REPS), Research Institute, King Fahd University of Petroleum & Minerals, (KFUPM), Dhahran 31261, Saudi Arabia*

Complete contact information is available at:
https://pubs.acs.org/10.1021/acsomega.2c02107

### Author Contributions

All authors have given approval to the final version of the manuscript.

### Notes

The authors declare no competing financial interest.

## ■ REFERENCES

(1) Kenisarin, M. M. Thermophysical Properties of Some Organic Phase Change Materials for Latent Heat Storage. A Review. *Sol. Energy* **2014**, *107*, 553−575.

(2) Zahir, M. H.; Irshad, K.; Aziz, M. A.; Shafiullah, M.; Rahman, M. M.; Hossain, M. M. Shape-Stabilized Phase Change Material for Solar Thermal Energy Storage: CaO Containing MgCO$_3$ Mixed with Polyethylene Glycol. *Energy Fuels* **2019**, *33*, 12041−12051.

(3) Zahir, M. H.; Rahman, M. M.; Irshad, K.; Rahman, M. M. Shape-Stabilized Phase Change Materials for Solar Energy Storage: MgO and Mg(OH)$_2$ Mixed with Polyethylene Glycol. *Nanomaterials* **2019**, *9*, 1773.

(4) Zahir, M.; Rahman, M. M.; Basamad, S. K. S.; Mohaisen, K. O.; Irshad, K.; Rahman, M. M.; Aziz, M. A.; Ali, A.; Hossain, M. M. Preparation of a Sustainable Shape Stabilized Phase Change Material for Thermal Energy Storage Based on Mg$^{2+}$ − Doped CaCO$_3$/PEG Composites. *Nanomaterials* **2021**, *11*, 1639.

(5) Farid, M. M.; Khudhair, A. M.; Razack, S. A. K.; Al-Hallaj, S. A Review on Phase Change Energy Storage: Materials and Applications. *Energy Convers. Manage.* **2004**, *45*, 1597−1615.

(6) Mohamed, S. A.; Al-Sulaiman, F. A.; Ibrahim, N. I.; Zahir, M. H.; Al-Ahmed, A.; Saidur, R.; Yılbaş, B. S.; Sahin, A. Z. A review on current status and challenges of inorganic phase change materials for thermal energy storage systems. *Renew. Sustain. Energy Rev.* **2017**, *70*, 1072−1089.

(7) Bakhtiari, A. B. S.; Hsiao, D.; Jin, G.; Gates, B. D.; Branda, N. R. An Efficient Method Based on the Photothermal Effect for the Release of Molecules from Metal Nanoparticle Surfaces. *Angew. Chem., Int. Ed.* **2009**, *48*, 4166−4169.

(8) Gole, J. L.; Burda, S. J. D.; Lou, C. Y.; Chen, X. Highly efficient formation of visible light tunable TiO$_{2-x}$N$_x$ photocatalysts and their transformation at the nanoscale. *J. Phys. Chem. B* **2004**, 1230−1240.

(9) Goh, E. G.; Xu, X.; McCormick, P. G. Effect of particle size on the UV absorbance of zinc oxide nanoparticles. *Acta Mater.* **2014**, *78-79*, 49−52.

(10) Umar, A.; Kumar, G.; Akhtar, M. S.; Wang, Y.; Kim, S. H. Ce-doped ZnO nanoparticles for efficient photocatalytic degradation of direct red-23 dye. *Ceram. Int.* **2015**, *4*, 7773−7782.

(11) Messih, M. F. A.; Shalan, A. E.; Sanad, M. F.; Ahmed, M. A. Facile approach to prepare ZnO@SiO$_2$ nanomaterials for photocatalytic degradation of some organic pollutant models. *J. Mater. Sci.: Mater. Electron.* **2019**, *30*, 14291−14299.

(12) Lai, C. Y.; Trewyn, B. G.; Jeftinija, D. M.; Jeftinija, K.; Xu, S.; Jeftinija, S.; Lin, V. S. Y. A mesoporous silica nanosphere-based carrier system with chemically removable CdS nanoparticle caps for stimuli-responsive controlled release of neurotransmitters and drug molecules. *J. Am. Chem. Soc.* **2003**, *125*, 4415−4459.

(13) Dixon, S. C.; Jiamprasertboon, A.; Carmalt, C. J.; Parkin, I. P. Luminescence behaviour and deposition of Sc$_2$O$_3$ thin films from scandium(III) acetylacetonate at ambient pressure. *Appl. Phys. Lett.* **2018**, *112*, 221902.

(14) Qian, T.; Li, J.; Ma, H.; Yang, J. The preparation of a green shape-stabilized composite phase change material of polyethylene glycol/SiO$_2$ with enhanced thermal performance based on oil shale ash via temperature-assisted sol−gel method. *Sol. Energy Mater. Sol. Cells* **2015**, *132*, 29−39.

(15) Li, B.; Dan, S.; Wang, R.; Zhai, L.; Yuye, C.; Lan, Y.; Cao, H.; Zou, C. Polyethylene glycol/silica (PEG@SiO$_2$) composite inspired by the synthesis of mesoporous materials as shape-stabilized phase change material for energy storage. *Renewable Energy* **2020**, *145*, 84−92.

(16) He, L.; Li, J.; Zhou, C.; Zhu, H.; Cao, X.; Tang, B. Phase change characteristics of shape-stabilized PEG/SiO2 composites using calcium chloride-assisted and temperature-assisted sol gel methods. *Sol. Energy* **2014**, *103*, 448−455.

(17) Li, J.; He, L.; Liu, T.; Cao, X.; Zhu, H. Preparation and characterization of PEG/SiO$_2$ composites as shape-stabilized phase change materials for thermal energy storage. *Sol. Energy Mater. Sol. Cells* **2013**, *118*, 48−53.

(18) Tang, B.; Qiu, M.; Zhang, S. Thermal conductivity enhancement of PEG/SiO$_2$ composite PCM by in situ Cu doping. *Sol. Energy Mater. Sol. Cells* **2012**, *105*, 242−248.

(19) Tang, B.; Wu, C.; Qiu, M.; Zhang, S.; Zhang, X. PEG/SiO$_2$-Al$_2$O$_3$ hybrid form-stable phase change materials with enhanced thermal conductivity. *Mater. Chem. Phys.* **2014**, *144*, 162−167.

(20) Tang, B.; Cui, J.; Wang, Y.; Jia, C.; Zhang, S. Facile synthesis and performances of PEG/SiO$_2$ composite form-stable phase change materials. *Sol. Energy* **2013**, *97*, 484−492.

(21) Zhang, Y.; Wang, J.; Qiu, J.; Jin, X.; Umair, M. M.; Lu, R.; Zhang, S.; Tang, B. Ag-Graphene/PEG Composite Phase Change Materials for Enhancing Solar-Thermal Energy Conversion and Storage Capacity. *Appl. Energy* **2019**, *237*, 83−90.

(22) Wang, W.; Yang, X.; Fang, Y.; Ding, J.; Yan, J. Preparation and thermal properties of polyethylene glycol/expanded graphite blends for energy storage. *Appl. Energy* **2009**, *86*, 1479−1483.

(23) Zahir, M.; Nagano, T. High-Selectivity Y$_2$O$_3$-Doped SiO$_2$ Nanocomposite Membranes for Gas Separation in Steam at High Temperatures. *J. Am. Ceram. Soc.* **2016**, 452−460.

(24) Zahir, M. H.; Sato, K.; Mori, H.; Iwamoto, Y.; Nomura, M.; Nakao, S. I. Preparation and Properties of Hydrothermally Stable g-alumina-Based Composite Mesoporous Membranes. *J. Am. Ceram. Soc.* **2006**, *89*, 2874−2880.

(25) Ikuhara, Y. H.; Mori, H.; Saito, T.; Iwamoto, Y. High-Temperature Hydrogen Adsorption Properties of Precursor-Derived Nickel Nanoparticle-Dispersed Amorphous Silica. *J. Am. Ceram. Soc.* **2007**, *90*, 546−552.

(26) Bouguerra, M.; Samah, M.; Belkhir, M. A.; Chergui, A.; Gerbous, L.; Nouet, G.; Chateigner, D.; Madelon, R. Intense photoluminescence of slightly doped ZnO−SiO$_2$ matrix. *Chem. Phys. Lett.* **2006**, *425*, 77−81.

(27) Cannas, C.; Mainas, M.; Musinu, A.; Piccaluga, G. ZnO/SiO$_2$ nanocomposites obtained by impregnation of mesoporous silica. *Compos. Sci. Technol.* **2003**, *63*, 1187−1191.

(28) Mao, H.; Li, B.; Li, X.; Liu, Z.; Ma, W. Mesoporous nickel (or cobolt)-doped silica-pillared clay: Synthesis and characterization studies. *Mater. Res. Bull.* **2009**, *44*, 1569−1575.

(29) Bhoware, S. S.; Singh, A. P. Characterization and catalytic activity of cobalt containing MCM-41prepared by direct hydrothermal, grafting and immobilization methods. *J. Mol. Catal. A: Chem.* **2007**, *266*, 118−130.

(30) Burattin, P.; Che, M.; Louis, C. Molecular Approach to the Mechanism of Deposition−Precipitation of the Ni(II) Phase on Silica. *J. Phys. Chem. B* **1998**, *102*, 2722−2732.

(31) Min, X.; Fang, M.; Huang, Z.; Liu, Y.; Huang, Y.; Wen, R.; Qian, T.; Wu, X. Enhanced thermal properties of novel shape-stabilized PEG composite phase change materials with radial mesoporous silica sphere for thermal energy storage. *Sci. Rep.* **2015**, *5*, 12964.

(32) Yang, J.; Zhou, J.; Nie, Z.; Liu, L. Preparation and Property Analysis of Phase Change Concrete PEG/SiO$_2$-CPCM. *Rev. Compos. Mater. Av.* **2019**, *29*, 21−26.

(33) Yan, D.; Ming, W.; Liu, S.; Yin, G.; Zhang, Y.; Tang, B.; Zhang, S. Polyethylene glycol (PEG)/silicon dioxide grafted aminopropyl group and carboxylic multi-walled carbon nanotubes (SAM) composite as phase change material for light-to-heat energy conversion and storage. *J. Energy Storage* **2021**, *36*, No. 102428.

(34) Cheng, L.; Lei, L.; Guo, S. R.; Zhu, C. G.; Rong, H. J.; Guo, D. W.; Zhang, L.; Jiang, Y.; Lin, J. J. Schistosoma japonicum: treatment of different developmental stages in mice with long-acting praziquantel implants. *Int. J. Pharm.* **2010**, *387*, 129−138.

(35) Yang, J.; Li, X.; Han, S.; Yang, R.; Min, P.; Yu, Z. Z. High-Quality Graphene Aerogels for Thermally Conductive Phase Change Composites with Excellent Shape Stability. *J. Mater. Chem. A* **2018**, *6*, 5880−5886.

(36) Yang, J.; Zhang, E.; Li, X.; Zhang, Y.; Qu, J.; Yu, Z. Z. Cellulose/graphene aerogel supported phase change composites with high thermal conductivity and good shape stability for thermal energy storage. *Carbon* **2016**, *98*, 50−57.

(37) Min, P.; Liu, J.; Li, X.; An, F.; Liu, P.; Shen, Y.; Koratkar, N.; Yu, Z.-Z. Thermally Conductive Phase Change Composites Featuring Anisotropic Graphene Aerogels for Real-Time and Fast-Charging Solar-Thermal Energy Conversion. *Adv. Funct. Mater.* **2018**, *28*, 1805365.

(38) Yang, J.; Li, X.; Han, S.; Zhang, Y.; Min, P.; Koratkar, N.; Yu, Z. Z. Air-dried, high-density graphene hybrid aerogels for phase change composites with exceptional thermal conductivity and shape stability. *J. Mater. Chem. A* **2016**, *4*, 18067−18074.